PHYSICAL REVIEW B VOLUME 46, NUMBER 15 15 OCTOBER 1992-I

Lateral-superlattice effect on weak localization in silicon inversion layers

J. R. Gao,* C. de Graaf, A. S. Schüssler, J. Caro, and S. Radelaar
Delft Institute of Microelectronics and Submicron Technology, Delft University of Technology, Lorentzweg 1, 2628 CJ Delft, The Netherlands

K. Heyers
Institute of Semiconductor Electronics, Aachen Technical University, D-5100 Aachen, Germany
(Received 1 June 1992)

It is found that the magnitude of the weak-localization (WL) correction to the conductance in a lateral superlattice (LSL) differs considerably from that in a homogeneous two-dimensional electron gas. The LSL effects were observed by measuring the dependence of the magnetoconductance on the strength of a modulated potential in silicon inversion layers. For parallel transport in a LSL the WL is enhanced, while it is reduced for perpendicular transport. This agrees with a recent theory for WL in a LSL. The effect is larger for stronger potential modulation and its maximum value deduced from the experiments is 2.8.

Three-dimensional (3D) semiconductor superlattices have been investigated intensively because of their unique properties and potential device applications since Esaki and Tsu[1] proposed such structures more than two decades ago. It was only recently, however, that Szott, Jedrzejek, and Kirk[2] calculated the weak-localization (WL) correction to the conductivity in such superlattices, taking into account the anisotropy of the electronic diffusion constant in the superlattice. A subsequent experimental study[3] demonstrated the correctness of their theory. Meanwhile, the theory was adapted for WL in a lateral superlattice (LSL),[4] the 2D equivalent of the Esaki and Tsu superlattice. This adapted theory shows that a LSL has similar effects on the WL as the 3D superlattice.

In this paper we report the experimental observation of superlattice effects in the weak localization of lateral superlattices. The effects were studied by measuring the low-field magnetoconductance (LFMC) of Si metal-oxide-semiconductor field-effect transistors (MOSFETs) as a function of the strength of the potential modulation in the inversion layer. Two types of superlattice MOSFETs were examined, the difference being the direction of the potential modulation with respect to the source-drain direction. In one type of device a crossover from 2D to 1D WL was induced by changing the operation mode from the LSL mode to the multiple quantum wire mode.

The devices used are dual-gate Si-MOSFETs fabricated on (100) wafers. Figure 1 shows a schematic cross section of a device, which is similar to that used by Warren, Antoniadis, and Smith.[5] The lower gate of the MOSFETs is a polysilicon grating of period $a=200$ nm. The direction of the grating lines, which are interconnected outside the channel area, depends on the type of device. In one type of device 240 grating lines are parallel to the source-drain (S-D) direction, covering a channel area $L\times W_{2D}=24\times 48\ \mu m^2$ (L is the channel length, W_{2D} is the 2D channel width). We call this device a LSL-0, since the angle between the grating lines and the S-D direction is zero degrees. In a LSL-90, the other type of device, 120 lines are perpendicular to the source-drain direction, covering the same channel area. In both cases the direction along the grating lines is defined as the x direction, while the direction of the potential modulation (perpendicular to the grating lines) is the y direction. The upper gate is a continuous aluminum layer.

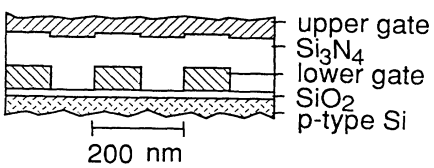

FIG. 1. Schematic cross section of a lateral superlattice MOSFET. The thickness of the gate oxide is 25 nm and that of the nitride 120 nm. The grating lines are 80 nm thick.

In a LSL-0 multiple quantum wires can be formed either by applying a voltage $V_{GU}>V_{GU,T}$ to the upper gate and a voltage $V_{GL}<V_{GL,T}$ to the lower gate ($V_{GU,T}$ and $V_{GL,T}$ are the threshold voltages for the gates), or by applying voltages $V_{GL}>V_{GL,T}$ and $V_{GU}<V_{GU,T}$ to the gates. In the first case quantum wires are formed under the gaps between the grating lines, while in the second case they are formed under the grating lines. Starting from either situation a 2D electron gas (2DEG) with a modulated surface potential, i.e., a LSL, can be formed by increasing the appropriate gate voltage to above threshold. The amplitude of the potential modulation is a function of both V_{GU} and V_{GL}. The same operation modes in principle apply to a LSL-90, but inducing multiple quantum wires is of no practical importance, since then the device does not conduct.

Figure 2 shows a family of LFMC traces of LSL-0 No. 1 taken between -0.12 and 0.12 T for $V_{GU}=28$ V and at a temperature $T=0.4$ K. The magnetic field was applied perpendicular to the plane of the sample. From device simulations[6] we expect that the V_{GL} values between -0.4 and 5.5 V cover an operation range from quantum wire mode via LSL mode to the homogeneous 2DEG mode. The last mode occurs only for one specific combination of

gate voltages. Beyond the 2DEG mode the system is again a LSL. In the quantum wire mode several (up to about five) 1D subbands are occupied.[7] For the field range shown in Fig. 2, the relative conductance increase amounts to 14% for $V_{GL}=-0.4$ V and this value gradually decreases to 1% for $V_{GL}=5.5$ V. This reduction cannot be described by a single functional form, since around $V_{GL}=0.6$ V also a clear change in the shape of the curves occurs (in addition to the disappearance of the negative magnetoconductance around zero field).

Our measurements give the magnitude of the change in conductance with field at a fixed temperature. Theoretically, for the 1D case[8] ($L_{in} > W_{1D}$, L_{in} being the inelastic diffusion length and W_{1D} the 1D channel width) this conductance change is

$$\Delta G(B)=G(B)-G(0)=\frac{N_c}{L}\frac{e^2}{\pi\hbar}n_v\alpha\left[L_{in}-\left(\frac{1}{L_{in}^2}+\frac{e^2W_{1D}^2B^2}{3\hbar^2}\right)^{-1/2}\right]. \quad (1)$$

For a LSL the conductance change for transport parallel and perpendicular to the equipotential lines of the superlattice is,[4] respectively,

$$\Delta G_x(B)=G_x(B)-G_x(0)$$
$$=\frac{W_{2D}}{L}\frac{e^2}{2\pi^2\hbar}n_v\alpha\left(\frac{D_x}{D_y}\right)^{1/2}\left[\Psi\left(\frac{1}{2}+\frac{\hbar}{4eB(D_xD_y)^{1/2}\tau_{in}}\right)-\ln\left(\frac{\hbar}{4eB(D_xD_y)^{1/2}\tau_{in}}\right)\right], \quad (2a)$$

$$\Delta G_y(B)=G_y(B)-G_y(0)=\frac{D_y}{D_x}\Delta G_x(B). \quad (2b)$$

Here $G(0)$ and $G(B)$ are the conductances at $B=0$ and $B\neq 0$. N_c is the number of quantum wires or 1D channels ($N_c=240$ for LSL-0), n_v is the valley degeneracy [$n_v=2$ for a (100) Si inversion layer] and α is an empirical constant depending on the relative magnitude of the inelastic scattering time τ_{in} and the intervalley impurity scattering time.[9] Ψ is the digamma function. Equations (2a) and (2b) are modifications of the usual expression for 2D weak localization in a homogeneous 2DEG for systems with an anisotropic diffusion constant D. In a LSL the component D_x parallel to the "channels" of the LSL exceeds the perpendicular component D_y and this inequality becomes stronger for stronger potential modulations. Thus, when compared to the homogeneous case, Eq. (2a) predicts an enhancement of the magnitude of the WL and Eq. (2b) a reduction. The magnitude of either of these effects increases with increasing potential modulation.

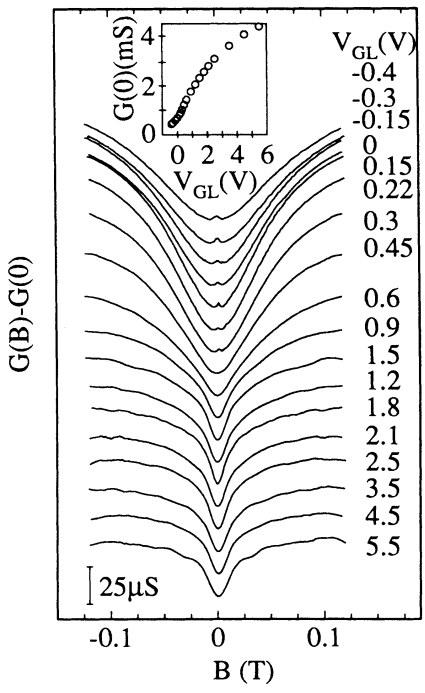

FIG. 2. Conductance of LSL-0 No. 1 as function of magnetic field for eighteen V_{GL} values and $V_{GU}=28$ V. The curves have a vertical offset. The inset shows a plot of the zero-field conductance $G(0)$ vs V_{GL}. $T=400$ mK.

To analyze whether in the modulated 2D case the LFMC shows the expected superlattice effects and to find the transition point between the 1D and 2D behavior, we fitted the above equations (1) and (2a) to the data of Fig. 2. However, the small negative magnetoconductance around $B=0$ for V_{GL} between -0.40 and 0.3 V is not described by Eqs. (1) and (2). Therefore, for these V_{GL} values the fits were made for the magnetic field range with a positive magnetoconductance.

Equation (1) was fitted in the magnetic field range determined by the condition $l_B \geq 1.2W_{1D}$ [$l_B=(\hbar/2eB)^{1/2}$ is the magnetic length] by adjusting W_{1D} and L_{in} and choosing $\alpha=0.3$, which is in the range of experimental values $\alpha=0.25$–0.35 reported in the literature.[10] The fitting of Eq. (2a) was done under the condition $l_B \gtrsim 1.6l_e$ ($l_e \approx 50$ nm is the elastic mean free path) and was simplified by making the identifications $L_{in,x}=(D_x\tau_{in})^{1/2}$ and $L_{in,y}=(D_y\tau_{in})^{1/2}$. Again α was set to 0.3. In this way $L_{in,x}$ and $L_{in,y}$ are the remaining fit parameters. We found that for $V_{GL} \leq 0.45$ V the data could only be fitted by Eq. (1), while for $V_{GL} \geq 0.60$ V only Eq. (2a) could describe the data. The fitted curves are almost indistinguishable from the data. Therefore, also in view of the values of the fit parameters to be discussed shortly, we conclude that multiple 1D channels are formed for $V_{GL} \leq 0.45$ V and for $V_{GL} \geq 0.60$ V the system follows the behavior of a LSL. In fact, the weak kink between 0 and 1 V in the plot of $G(0)$ vs V_{GL}, which is shown in the inset of Fig. 2, already gives an indication of the change of

operation mode deduced from the fitting results.

The prefactor $(D_x/D_y)^{1/2}$ of Eq. (2a) and the inelastic diffusion lengths $L_{in,x}$ and $L_{in,y}$, deduced from the fitting procedure, are plotted as a function of V_{GL} in Figs. 3(a) and 3(b). It is evident that superlattice effects enhance the WL considerably (up to a factor of 2.8). For the strongest potential modulation the enhancement factor $(D_x/D_y)^{1/2}$ is at its maximum. With decreasing modulation, i.e., increasing V_{GL}, the enhancement decreases and finally saturates at a value of approximately unity above 2.5 V. By definition, the saturation corresponds to a very weak potential modulation or a virtually homogeneous 2DEG. The values of $L_{in,x}$ and $L_{in,y}$ are in the range expected for our MOSFETs. The dependence of $L_{in,x}=(D_x\tau_{in})^{1/2}$ and $L_{in,y}=(D_y\tau_{in})^{1/2}$ on V_{GL} ($\propto \bar{n}_s$, the average electron density) can be understood from the dependences of $D_x \propto (v_{F,x})^2\tau_e$, $D_y \propto (v_{F,y})^2\tau_e$ and τ_{in} on $\bar{n}_s$. To the left of the maxima of the curves the proportionality of v_F^2 and τ_{in} to $\bar{n}_s$ dominates. We speculate that to the right of the maxima this proportionality is overruled by a decrease of τ_e due to increased interface roughness scattering at high gate voltages (stronger 2D confinement). In the range of saturation of $(D_x/D_y)^{1/2}$ the difference between the LSL and a homogeneous 2DEG is small, so that $L_{in,x}$ and $L_{in,y}$ are approximately equal.

In the multiple quantum wire mode the values of L_{in} [see Fig. 3(b)] fall in a relatively narrow band and always exceed W_{1D}, which justifies the use of Eq. (1). At the transition point between 1D and 2D WL the curve which describes the average behavior of L_{in} lines up with $L_{in,x}$ just across the transition point, as to be expected. On the average L_{in} in the 1D regime is smaller than $L_{in,x}$ and $L_{in,y}$ in the regime of weak potential modulations. This agrees qualitatively with experimental data of Wheeler *et al.*[11] deduced from WL experiments on 1D and 2D MOSFETs. W_{1D} [see Fig. 3(a)] increases with V_{GL}, as can be understood from electrostatic considerations. For

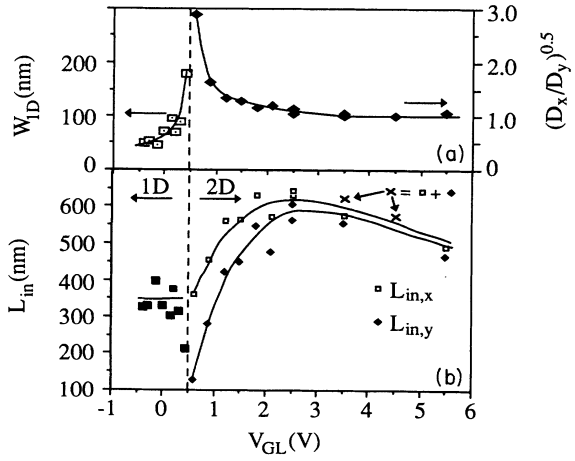

FIG. 3. Parameters deduced from fits of Eqs. (1) and (2) to the data of Fig. 2: (a) W_{1D} and $(D_x/D_y)^{1/2}$ and (b) L_{in} for the 1D case, and $L_{in,x}$ and $L_{in,y}$ for the LSL case. The dashed vertical line denotes the transition point between 1D and 2D behavior.

$V_{GL}=0.45$ V the fitted W_{1D} is 180 nm, which exceeds the gap width between the grating lines. We attribute this effect to breakdown of the 1D WL theory close to the transition from quantum wires to superlattice. The deviating behavior of L_{in} for $V_{GL}=0.45$ V is explained in the same way.

The negative magnetoconductance around $B=0$ occurring in Fig. 2 for $V_{GL}\leq 0.3$ V resembles spin-orbit (SO) scattering effects observed in the WL of metal films[12,13] and of the 2DEG in a GaAs/AlGaAs heterojunction.[14] We observed this effect in all the LSL-0 devices measured, sometimes also in the LSL mode, and in a number of LSL-90 devices. The amplitude of the peak decreases strongly with increasing temperature, so that it becomes indiscernible from the noise above 400 mK. In an attempt to analyze the negative magnetoconductance we used modified versions[13,15] of Eqs. (1) and (2) to describe the effect of SO scattering in the electron gas in a MOSFET. A mechanism which might give rise to such an effect is the D'yakonov-Perel' mechanism.[16] It was not possible, however, to obtain acceptable fits using these modified equations. The proper description of the negative magnetoconductance thus remains to be clarified.

In connection with the transition from 1D to 2D behavior, we note that the prefactor $(D_x/D_y)^{1/2}$ is a kind of interpolation factor. This can for instance be seen from the property[4] that, due to the presence of the prefactor, the $B=0$ equivalent of Eq. (2a) in the limit $D_y\rightarrow 0$ (decoupled wires) goes over into the $B=0$ equivalent of Eq. (1). In the regime of increasingly strong potential modulation the dispersion relation $E(k_y)$ is a set of increasingly flattening minibands, which corresponds to a low electron velocity and a low diffusion coefficient in the y direction. In the limit $D_y\rightarrow 0$ the minibands transform to the dispersionless energy levels characteristic of quantum wires. Then the WL behavior is 1D, which is stronger than 2D behavior.

In order to explore further the superlattice effects, we measured LFMC traces of device LSL-90 No. 1 at 0.3 K for $V_{GL}=4$ V and for V_{GU} between -7 and 15 V. In this range of gate biases the amplitude of the potential modulation decreases from strong to very weak. For comparison the LFMC of LSL-0 No. 2 was also measured for gate biases in the same range. A selection of measured curves is shown in Fig. 4. Clearly, V_{GU} has a strong influence on the magnitude of the LFMC. There is a difference, however, between the two devices. For LSL-90 No. 1, ΔG_y decreases strongly with increasing V_{GU} in the whole field range, while for LSL-0 No. 2 on the contrary ΔG_x increases with V_{GU} at low fields, but shows the opposite behavior for the higher fields. We fitted Eqs. (2a) and (2b) to the data of Fig. 4 in the way already described. Figure 5 shows the dependence on V_{GU} of the resulting prefactors $(D_x/D_y)^{1/2}$ and $(D_y/D_x)^{1/2}$ of ΔG_x and ΔG_y, respectively. The overall behavior of the prefactors is in agreement with the theory. In principle the prefactors should be reciprocal to each other. Although this is not exactly the case, we think the correspondence is still quite good, especially when one takes into account that the two devices come from different wafers.

The WL behavior of LSL-0 No. 1 and LSL-90 No. 2

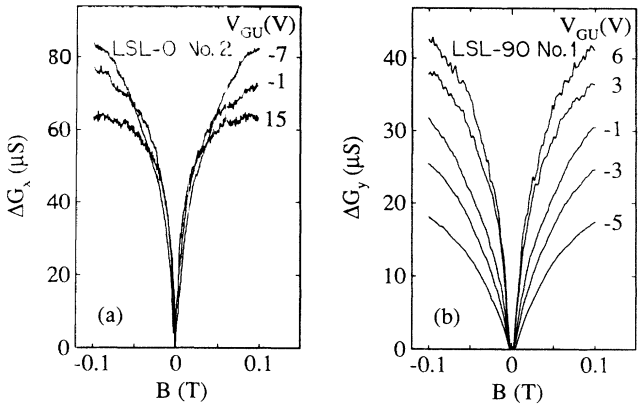

FIG. 4. Low-field magnetoconductance (a) ΔG_x of LSL-0 No. 2 and (b) ΔGy of LSL-90 No. 1. $V_{GL}=4$ V and the V_{GU} values are indicated in the figures. $T=300$ mK.

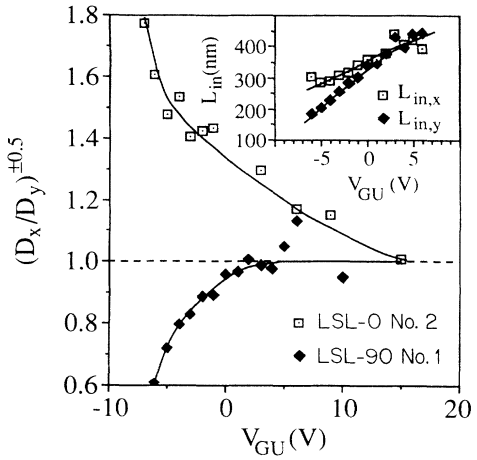

FIG. 5. $(D_x/D_y)^{1/2}$ (LSL-0 No. 2) and $(D_y/D_x)^{1/2}$ (LSL-90 No. 1) deduced from fits of Eqs. (2) to the LFMC curves in Fig. 4. The lines are guides to the eye. The inset shows the V_{GU} dependence of $L_{in,x}$ and $L_{in,y}$ for LSL-90 No. 1.

can now be understood as follows. For LSL-90 No. 1 the inelastic lengths increase with increasing V_{GU}, so that the characteristic width of the LFMC curves decrease with V_{GU}, whereas their amplitude increases. At the same time $(D_y/D_x)^{1/2}$ increases. The result is the sequence of nested curves of Fig. 4(b). For LSL-0 No. 2 the increase of the inelastic lengths dominates at low V_{GU}, but the decrease of $(D_x/D_y)^{1/2}$ determines the behavior for high V_{GU}. This explains the crossing of the curves in Fig. 4(a). From the device simulations mentioned before, we expect, if the range of gate biases in Fig. 5 is wide enough, that for some positive V_{GU} a homogeneous 2DEG is induced and beyond this again a LSL. From Eqs. (2) we therefore expect a minimum to occur in the $(D_x/D_y)^{1/2}$ curve for this value of V_{GU}, and a maximum in the $(D_y/D_x)^{1/2}$ curve. However, this feature is not borne out by the data, probably because at the higher gate voltages the potential modulation is too weak to have a substantial influence on the conductance. The absence of a minimum in the $(D_x/D_y)^{1/2}$ curve of Fig. 3(a) can be understood in a similar way. In the inset of Fig. 5 we have plotted $L_{in,x}$ and $L_{in,y}$ of LSL-90 No. 1 as a function of V_{GU}. Due to the smaller V_{GU} applied to LSL-90 No. 1, its values of $L_{in,x}$ and $L_{in,y}$ are smaller than those of LSL-0 No. 1 at $V_{GL}=4$ V [see Fig. 3(b)]. Like in the low-density regime of a homogeneous electron gas the inelastic lengths increase with gate voltage (average electron density), but at different rates. Above $V_{GU}=2$ V the clear distinction between the behavior of $L_{in,x}$ and $L_{in,y}$ is lost. This range corresponds to a virtually homogeneous electron gas.

In summary, we have observed, for the first time, lateral superlattice effects in the weak localization by measuring the magnetoconductance of superlattice MOSFETs. In qualitative agreement with a recent theory of such effects, the WL is enhanced for parallel transport in a lateral superlattice and reduced for perpendicular transport. The magnitude of the effect increases with increasing potential modulation. In one type of device we induced a crossover from 2D WL in the superlattice mode to 1D WL in the quantum wire mode.

We thank W. Szott and S. Feng for their comments on the manuscript and R. G. Wheeler for useful discussions. This work is part of the research program of the Stichting Fundamenteel Onderzoek der Materie (FOM), which is financially supported by the Nederlandse Organisatie voor Wetenschappelijk Onderzoek (NWO).

*Present address: Laboratory of Applied Physics, Groningen University, Nijenborgh 18, 9747 AG Groningen, The Netherlands.

[1]L. Esaki and R. Tsu, IBM J. Res. Dev. **14**, 61 (1970).

[2]W. Szott, C. Jedrzejek, and W. P. Kirk, Phys. Rev. B **40**, 1790 (1988).

[3]W. Szott, C. Jedrzejek, and W. P. Kirk, Phys. Rev. Lett. **63**, 1980 (1989).

[4]W. Szott, C. Jedrzejek, and W. P. Kirk, Superlattices Microstruct. **11**, 199 (1992).

[5]A. C. Warren, D. A. Antoniadis, and H. I. Smith, Phys. Rev. Lett. **56**, 1858 (1986).

[6]Device simulations were performed using PISCES-2B, Two Dimensional Device Analysis Program, Version 8908, Technology Modeling Associates, Inc., 1989 (unpublished).

[7]J. R. Gao, C. de Graaf, J. Caro, S. Radelaar, M. Offenberg, V. Lauer, J. Singleton, T. J. B. M. Janssen, and J. A. A. J. Perenboom, Phys. Rev. B **41**, 12315 (1990).

[8]B. L. Al'tshuler and A. G. Aronov, Pis'ma Zh. Eksp. Theor. Fiz. **33**, 515 (1981) [JETP Lett. **33**, 499 (1981)].

[9]H. Fukuyama, Surf. Sci. **113**, 489 (1982).

[10]See, for example, N. Paquin, M. Pepper, A. Gundlach, and A. Ruthven, Phys. Rev. B **38**, 1593 (1988).

[11]R. G. Wheeler, K. K. Choi, A. Goel, R. Wisnieff, and D. E. Prober, Phys. Rev. Lett. **49**, 1674 (1982).

[12]G. Bergmann, Phys. Rep. **101**, 1 (1984).

[13]P. Santhanam, S. Wind, and D. E. Prober, Phys. Rev. Lett. **53**, 1179 (1984).

[14]P. D. Dresselhaus, C. M. A. Papavassilious, and R. G. Wheeler, Phys. Rev. Lett. **68**, 106 (1982).

[15]S. Hikami, A. Larkin, and Y. Nagaoka, Prog. Theor. Phys. **63**, 707 (1980).

[16]M. I. D'yakonov and V. I. Perel', Zh. Eksp. Theor. Fiz. **60**, 1954 (1971) [Sov. Phys. JETP **33**, 1053 (1971)].